AFWL-TR-77-274

(2) LEVEL II

FRACTURE ANALYSIS OF REENTRY VEHICLE STRUCTURAL MATERIALS

September 1978

Final Report

Approved for public release; distribution unlimited.

AIR FORCE WEAPONS LABORATORY
Air Force Systems Command
Kirtland Air Force Base, NM 87117

AFWL-TR-77-274

This final report was prepared by the Air Force Weapons Laboratory, Kirtland Air Force Base, New Mexico, Job Order 88090806. Major C. D. Stuber(DYV) was the Laboratory Project Officer-in-Charge.

When US Government drawings, specifications, or other data are used for any purpose other than a definitely related Government procurement operation, the Government thereby incurs no responsibility nor any obligation whatsoever, and the fact that the Government may have formulated, furnished, or in any way supplied the said drawings, specifications, or other data is not to be regarded by implication or otherwise as in any manner licensing the holder or any other person or corporation or conveying any rights or permission to manufacture, use, or sell any patented invention that may in any way be related thereto.

This report has been authored by an employee of the United States Government. Accordingly, the United States Government retains a nonexclusive, royalty-free license to publish or reproduce the material contained herein or allow others to do so, for the United States Government purposes.

This report has been reviewed by the Office of Information (OI) and is releasable to the National Technical Information Service (NTIS). At NTIS, it will be available to the general public, including foreign nations.

This technical report has been reviewed and is approved for publication.

JEFFREY A YAKER
1LT, USAF
Project Officer

FOR THE COMMANDER

DERMOD KELLEHER
Chief, Environment and Effects Branch

THOMAS W. CIAMBRONE
Lt Colonel, USAF
Chief, Applied Physics Division

DO NOT RETURN THIS COPY. RETAIN OR DESTROY

UNCLASSIFIED

SECURITY CLASSIFICATION OF THIS PAGE (When Data Entered)

REPORT DOCUMENTATION PAGE

READ INSTRUCTIONS BEFORE COMPLETING FORM

1. REPORT NUMBER: AFWL-TR-77-274
2. GOVT ACCESSION NO.
3. RECIPIENT'S CATALOG NUMBER
4. TITLE (and Subtitle): FRACTURE ANALYSIS OF REENTRY VEHICLE STRUCTURAL MATERIALS
5. TYPE OF REPORT & PERIOD COVERED: Final Report
6. PERFORMING ORG. REPORT NUMBER
7. AUTHOR(s): C. D. Stuber, Major, USAF
8. CONTRACT OR GRANT NUMBER(s)
9. PERFORMING ORGANIZATION NAME AND ADDRESS: Air Force Weapons Laboratory (DYV) Kirtland Air Force Base, NM 87117
10. PROGRAM ELEMENT, PROJECT, TASK AREA & WORK UNIT NUMBERS: 62601F; 88990806; 11 09
11. CONTROLLING OFFICE NAME AND ADDRESS: Air Force Weapons Laboratory (DYV) Kirtland Air Force Base, NM 87117
12. REPORT DATE: Sept[illegible] 1978
13. NUMBER OF PAGES: 58; 61p.
14. MONITORING AGENCY NAME & ADDRESS (if different from Controlling Office): SBIE; AD E200 234
15. SECURITY CLASS. (of this report): UNCLASSIFIED
15a. DECLASSIFICATION DOWNGRADING SCHEDULE
16. DISTRIBUTION STATEMENT (of this Report)

Approved for public release; distribution unlimited.

17. DISTRIBUTION STATEMENT (of the abstract entered in Block 20, if different from Report)
18. SUPPLEMENTARY NOTES
19. KEY WORDS (Continue on reverse side if necessary and identify by block number)

Composite Materials	Fractography	Flexure Properties
Carbon Phenolic Materials	Degradation	Strain Rate
Quartz Phenolic Materials	Dynamic Fracture	Flyer Rates
Graphite Epoxy	Dynamic Tests	

20. ABSTRACT (Continue on reverse side if necessary and identify by block number)

Fractography and analysis was performed on specimens of three dimensional quartz phenolic (3DQP), graphite/epoxy (G/E) composite, and tape wrapped carbon phenolic (TWCP) materials. These specimens had been fractured under well characterized test conditions and the pretest condition of the materials was well known in all cases. The fractography was correlated with the test results to see what effect, if any, that testing at various strain rates and preconditioning of the materials had on the fracture appearance of these materials. The fractography (over)

DD FORM 1 JAN 73 1473 EDITION OF 1 NOV 65 IS OBSOLETE

UNCLASSIFIED

SECURITY CLASSIFICATION OF THIS PAGE (When Data Entered)

20. ABSTRACT (Cont'd)

correlated well with the test results. When a strain rate effect or a preconditioning effect was observed in the test results, there was also a different appearance in the fracture surfaces.

A

SUMMARY

Fractography and analysis was performed on specimens of three-dimensional quartz phenolic (3DQP), graphite/epoxy (G/E) composite material, and tape wrapped carbon phenolic (TWCP) material. These specimens had been fractured under well characterized test conditions and the pretest condition of the materials was well known in all cases. The fractography was correlated with the test results to see what effect, if any, that testing at various strain rates and preconditioning of the material had on the fracture appearance of these materials.

The 3DQP material, which had a significant strain rate sensitivity, also fractured in a significantly different manner when tested at high strain rates compared to static tests. Macroscopically, more transverse shear was observed in the specimens which were tested dynamically, and microscopically, these specimens showed a much finer structure in the fracture surfaces of the resin pockets.

The particular graphite/epoxy material used in this program had little differences in the fracture surface, regardless of strain rate at which it was tested and the degree to which it was degraded before test. No differences could be detected microscopically and a somewhat finer declamination was observed on the "Circumferential" orientation specimens when tested at high strain rates. This correlated very well with the test results.

The TWCP materials had little difference in the appearance of the specimens tested statically compared with those tested dynamically, either microscopically or macroscopically, which agreed with the test results. Although there was no microscopic difference in the fracture surfaces of virgin material compared to degraded material, the angle at which fracture occurred on the "axial" orientation specimens was different between the preconditioned and virgin materials. This could explain the difference in the test results which was observed, i.e., the degraded material had less strength.

PREFACE

This report covers one task of the Dynamic/Degraded Properties (DDP) Program. Three other tasks of this program were done under contract (funded by AFWL through project orders) from SAMSO/ABRES to Effects Technology, Inc., Santa Barbara, California and are reported in SAMSO-TR-77-90, Vol. 15, "Dynamic and Degraded Properties of Reentry Materials" by R. Globus, K. VanBlaricum, and R. Parisse, all of Effects Technology, Inc. The need for the DDP Program was suggested by the Nuclear Hardness Evaluation Procedures (NHEP) Program, a joint Air Force-Defense Nuclear Agency program being technically directed at AFWL.

The author wishes to gratefully acknowledge Mr Charles J Miglionico, AFWL/DYV, Materials Science Group, for all of the excellent Scanning Electron Microscopy and his technical advice which enabled the timely completion of this program.

CONTENTS

SECTION I

INTRODUCTION

The dynamic/degraded properties program was devised to look at the properties of various candidate reentry vehicle materials after they had been degraded in a simulated nuclear radiation (X-ray) exposure. Also the effect of high strain rate loading on the properties of these materials was examined. Currently, most designers use material properties that were determined by conducting mechanical tests on virgin materials at very low strain rates, usually referred to as "static" tests. Such data are usually readily available (see ref. 1 and 2). However, in service, the critical loads often occur as dynamic loads or at very high strain rates. In order to understand the one-dimensional shock response of these materials, considerable work has been done in gas gun and magnetic flyer impact facilities which loads the material at extremely high strain rates, in the order of 10^5 cm/cm/sec or higher (see ref. 3, 4, and 5). This, however, gives little data on structural properties where strain rates seldom exceed 10×10^3 cm/cm/sec. Thus, there is a broad gap between static properties (where testing is usually done at strain rates of 10^{-3} cm/cm/sec or lower) and the impact properties. This program attempts to fill this technology gap and to determine the importance of these properties to reentry vehicle designers.

The second major area that was investigated in this program was the mechanical properties of materials that had been damaged in a simulated nuclear encounter. When one looks at the scenario of a typical reentry vehicle mission, any potential X-ray encounter would occur prior to reentry. Thus, the aerodynamic loads of reentry will occur after any damage from the nuclear encounter. This portion of the program investigated the properties of materials that had been exposed to a simulated nuclear encounter to check that there was sufficient residual strength left in the material for the reentry vehicle to survive the aerodynamic forces of reentry.

This program was organized into four major tasks. These were:

1. Materials Testing - - Conduct static and dynamic tests on virgin, and damaged materials.

2. Analysis - - Using data generated in the above task, identify failure modes, define failure criteria and determine critical properties.

3. RV Hardness Assessment - - Assess the applicability of data generated to RV nuclear V&H determination.

4. Fracture Analysis - - Determine the modes of failure through fractography analysis.

The first three of the above tasks were performed under an Air Force Contract with Effects Technology, Inc. and the results of these tasks are reported in SAMSO TR-77-90 Vol. 15 (ref. 6). The fourth task was performed in-house at the Air Force Weapons Laboratory (AFWL) and is reported in here.

There has not been much work reported in the way of fractography on reentry vehicle materials. However, there has been some very interesting work which studied the impact properties of hybrid composites (ref. 7, 8 and 9). In this work, a considerable amount of fractography (including SEM fractographs) was reported.

This task used the same specimens as those used in the Materials Testing Task (results published in ref. 6). These materials are: (1) three dimensional quartz phenolic (3DQP), (2) tape wrapped carbon phenolic, and (3) graphite/epoxy (G/E) composite material. The 3DQP specimens were all cut from rings which were 21.6 cm diameter x 5.1 cm long. The material was produced by Fiber Materials, Inc. The G/E composite material consisted of 22 plies of T300/5208 of $[90_3/0_2/90_4/0/\pm45/0/90_4/0_2/90_3]$. The TWCP material was HITCO flat molded FM5822A material layed up at a ply orientation of 20 degrees.

The specimens were carefully examined visually and with low power optical microscopy before they were mechanically tested. This was used primarily to determine the consistency and to a lesser extent, the quality of the material used in the program. Low power microscopy was also used to determine the extent of damage in the degraded materials, i.e., look for microcracks that might be present in the material before it was subjected to the three point bend tests.

After the three point bend test (results of which are reported in ref. 6), the specimens were carefully examined visually, with low power [illegible] scopy, and with the scanning electron microscope (SEM). [illegible] any differences between like specimens that were tested [illegible] tested dynamically and between specimens made of virgin [illegible]

made of degraded material. With optical means, magnifications from 2X to 20X were found to be most useful and are referred to as "macroscopic" examinations in this report. Similarly, magnifications of 200X to 2000X were found to be the most useful in the SEM and these results are referred to as "microscopic" examinations.

SECTION II

THREE DIMENSIONAL QUARTZ PHENOLIC (3DQP) MATERIAL

The 3DQP specimens were examined before testing by visual examination and low power microscopy. The density of the specimens was also measured. The specimens used for testing were cut from two different rings of material which had supposedly been fabricated by the same process and by the same technique. This material varied considerably from sample to sample and from ring to ring. Samples cut from the first ring were significantly different from the samples cut from the second ring.

3DQP material consists of bundles of quartz fibers which are impregnated with resin arranged in a three dimensional weave. Resin fills the voids in between the bundles of fibers. Examination of this material revealed that frequently the voids between the fiber bundles was not completely full of resin and occasionally had very little resin in the voids. Another significant observation was that the fiber bundles were not always straight. They either buckled or were nonorthogonal to each other. Photographs of this material are shown in figure 1. The voids described above are clearly visible in figure 1b. Since all of the specimens were cut from rings, the specimens cut in "circumferential" orientation were arc segments rather than straight. Actually, the "axial" specimens were also arcs, but the curve was across the width rather than the length.

The density measurements on the 3DQP revealed the inhomogenity of this material. Specimens cut from one ring ranged from 1.63 to 1.66 g/cc density with an average of 1.65 g/cc. Specimens cut from the second ring ranged from 1.65 to 1.69 g/cc with an average density of 1.68 g/cc.

Figures 2 and 3 are photographs of the 3DQP specimens after test. As can be seen, the specimens subjected to dynamic testing ($\dot{\varepsilon} = 10^{2}$ cm/cm/sec) failed with somewhat more transverse shear. Fiber and fiber bundle pull-out was rather extensive on all the specimens and most of the specimens hung together after test by the intertwining of pulled out fibers.

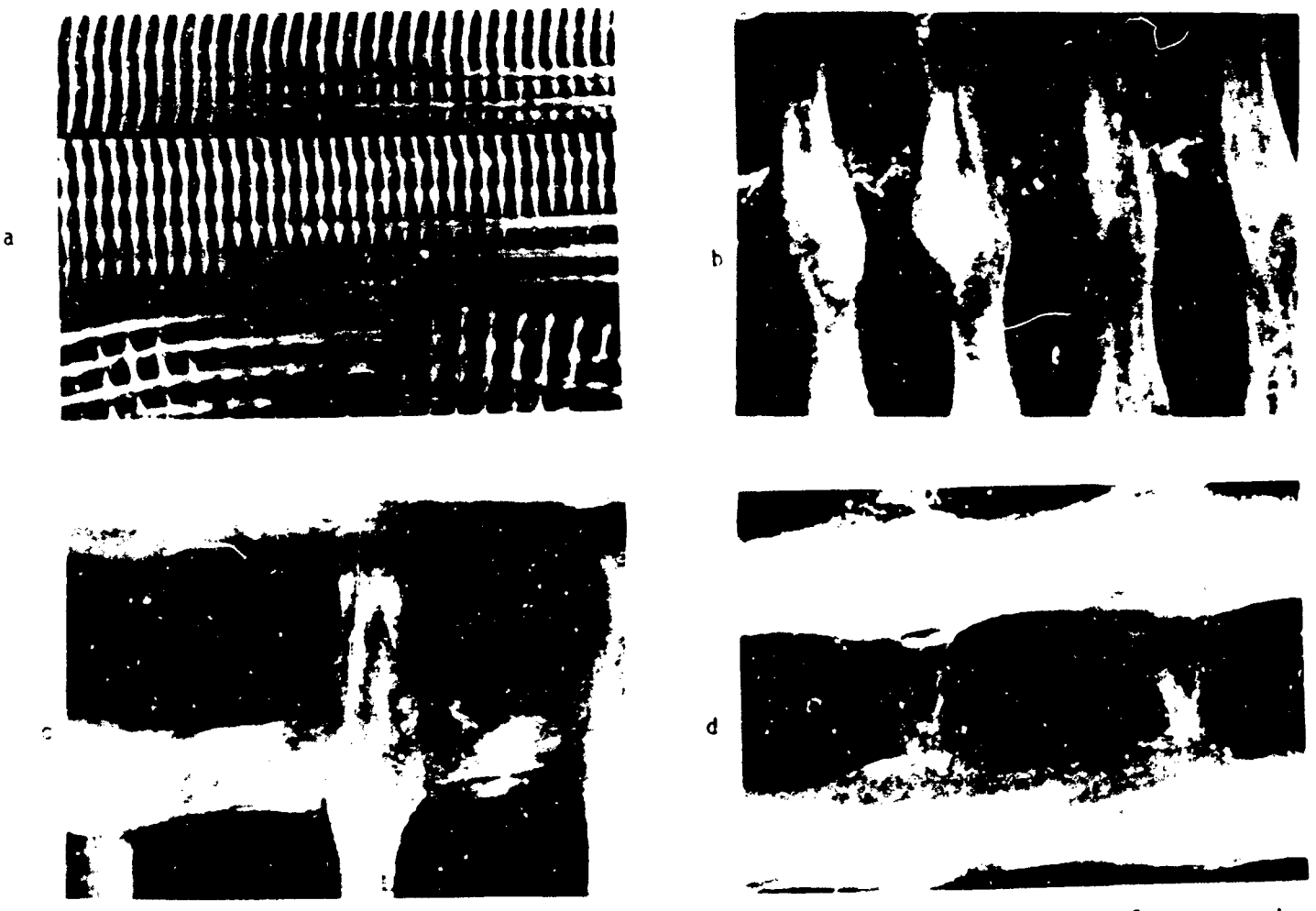

Figure 1. Macroscopic Views of 3DQP Specimens. (a) Upper two specimens were cut from same ring at two different orientations; bottom specimen cut from different ring 2X. (b) Middle specimen 20X. (c) Bottom specimen 20X. (d) Upper specimen 20X.

The 3DQP fracture surfaces were examined with the scanning electron microscope (SEM). Some of the photomicrographs taken with the SEM are shown in figures 4 and 5. Figures 4a and b and 5a and b were taken during a preliminary examination of the fracture surfaces and it was noted that the specimens which had been tested dynamically showed a much finer fracture pattern in the resin areas at high magnifications (compare figure 4b with figure 5b). Since low power photomicrographs of specimens did not appear much different (figures 4a and 5a), it was thought that the high power pictures might have been coincidental and were not representative. Thus, several additional specimens from both those that had been statically tested and those that had been dynamically tested were examined closely for this feature and it was found that those that had been tested dynamically consistently had a much finer fracture pattern in the resin areas compared with those which had been tested statically. Figures 4c and 4d of "static" tests and figures 5c and 5d of "dynamic" tests are other areas which clearly show this difference. No significant differences could be detected in the fiber areas of the specimens.

Two completely different and unrelated explanations are offered to account for this difference in the appearance of the fracture surface in the resin areas of the 3DQP when tested at these different strain rates. The first is that the resin, being a polymeric material, behaves like a viscous material, at least on the microscopic scale. Thus, when this material is loaded at a very low strain rate, i.e., static loading, the flaws or cracks in the material grow by a viscous flow or separation at the tip of the crack. Instead of a sharp crack propagating rapidly by a cleavage-like process, a blunt crack tip propagates by a flow of the material at the tip. This viscous flow leaves the relatively smooth fracture surface that was observed on the statically tested specimens. On the other hand, when the material is strained at a high strain rate, there is insufficient time for the necessary viscous flow and the resin fractures by the rapid propagation of all the flaws which are of the proper orientation and of sufficient size. These cracks then run together to produce the overall fracture surface on the resin pockets. It is the rapid propagation and joining of these cracks that give the fine structure of the fracture surface of the resin in the specimens which were tested dynamically.

The second explanation assumes that fracture occurs in the resin by rapid crack propagation in both the static case and the dynamic case. This assumes that the static fracture toughness is less than the dynamic fracture toughness

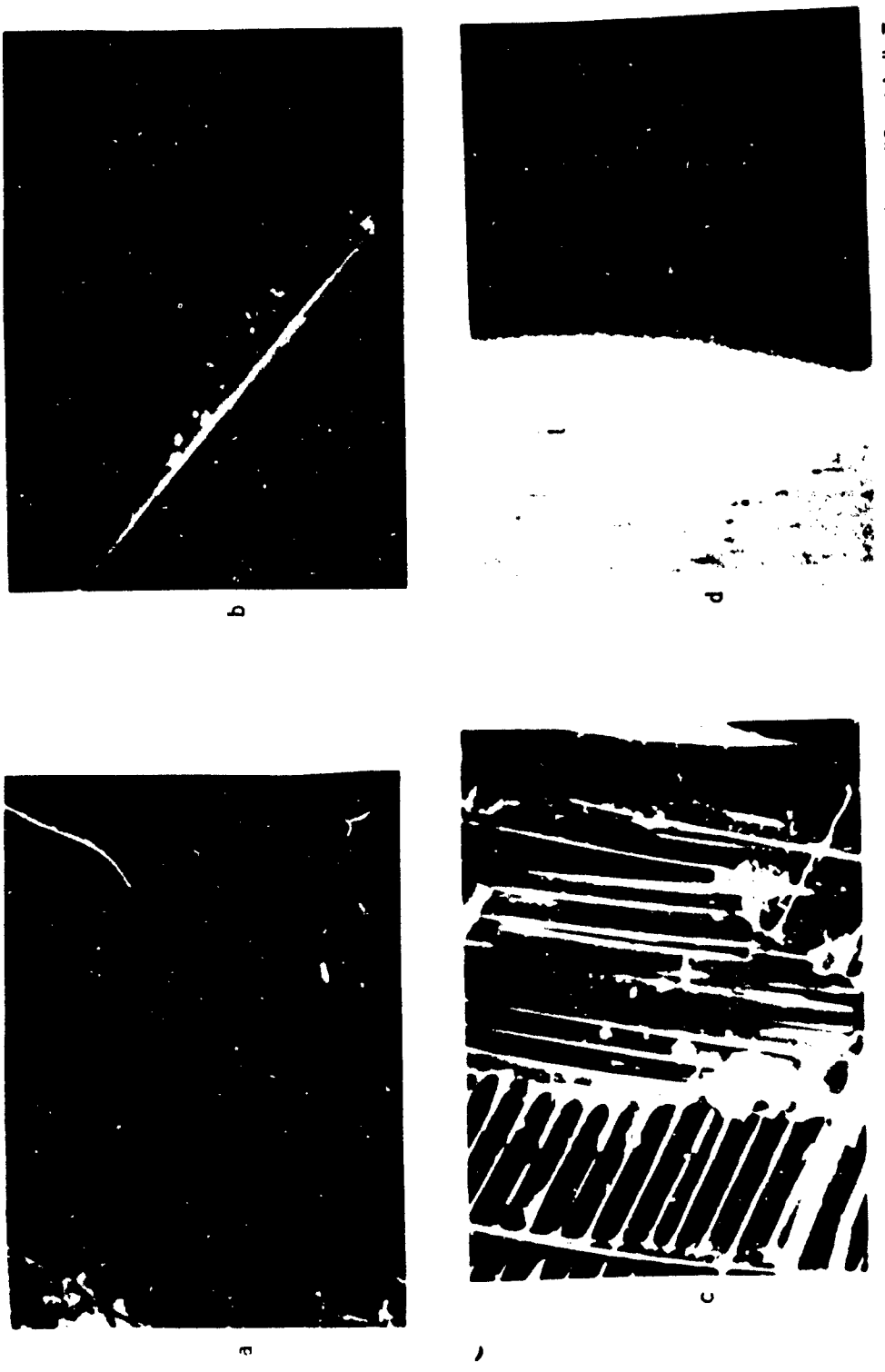

Figure 4. Microscopic (SEM) Views of Resin Pockets in the Fracture Surfaces of 3DQP after "Static" Tests. (a) First area 110X. (b) First area 200X. (c) Second area 500X. (d) Third area 1000X.

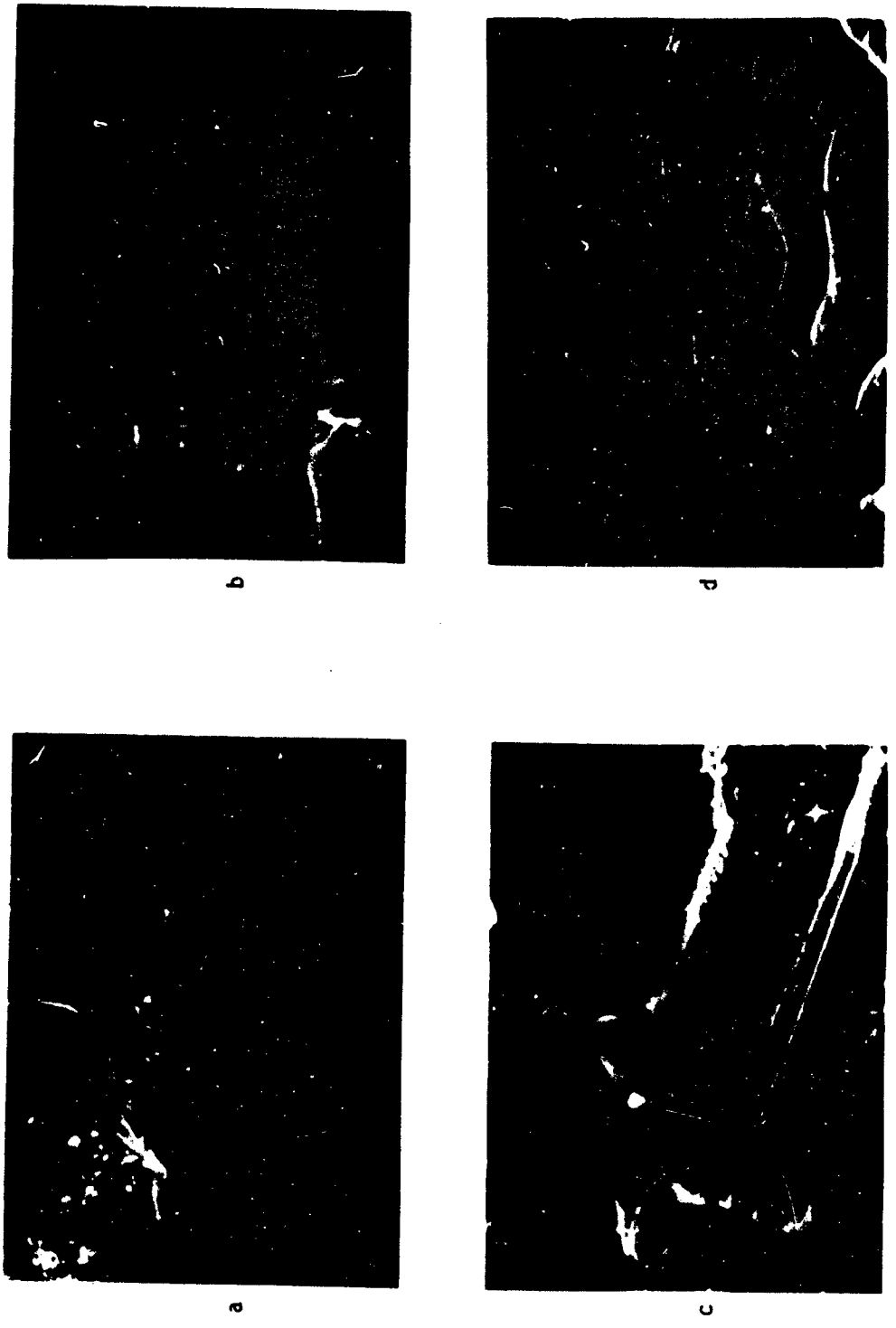

Figure 5. Microscopic (SEM) Views of Resin Pockets in the Fracture Surfaces of 3D9P after "Dynamic" Tests. (a) First area 200X. (b) First area 2000X. (c) Second area 500X. (d) Third area 2000X.

and consequently, the existing flaws in the material are sufficient to cause critical crack growth when the material is tested statically and thus a single critical flaw propagates across the resin pocket in a cleavage-like manner and causes the relatively smooth surface. On the other hand, when the material is tested dynamically, a number of the existing flaws grow (since none of the flaws are of critical size) until at least one becomes critical size. Thus, the fine fracture structure observed in the dynamic tests is caused by the multiple crack growth.

SECTION III

EXAMINATION OF VIRGIN GRAPHITE/EPOXY (G/E) AND TAPE WRAPPED CARBON PHENOLIC (TWCP) MATERIAL

A number of the virgin G/E and TWCP specimens were examined both visually and with low power optical microscopy before the three point bend tests were conducted. A sample of each material was also viewed in the SEM.

Nearly all of the G/E had scattered voids. Typical examples are shown in figure 6. On many of the G/E specimens, boundaries between individual plies could be observed. This can be seen in figure 7. These boundary areas appear to be rich in matrix. These boundaries were readily apparent when viewed in a small bench microscope, even without a fine polish. However, in order to photograph this phenomenon in a metallograph, the surfaces had to be polished to 1 micron grit and even then were not so readily apparent. Samples of G/E were also viewed in the scanning electron microscope. SEM photomicrographs are shown in figure 8.

All of the TWCP samples examined were very uniform. Examples of TWCP are shown in figure 9 and these are quite representative of all the TWCP. The SEM was also used to view the TWCP. SEM photomicrographs are shown in figure 10.

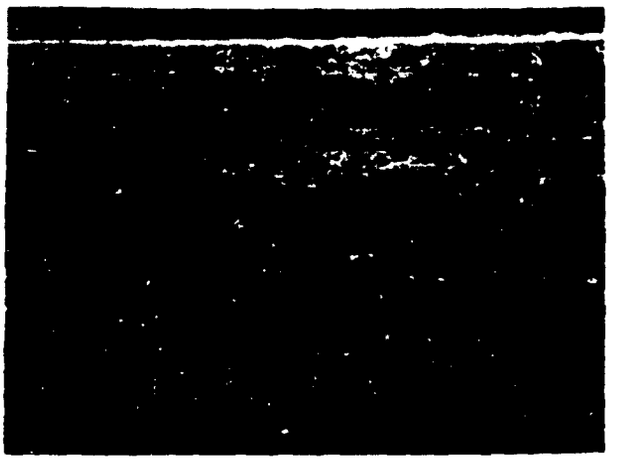

a

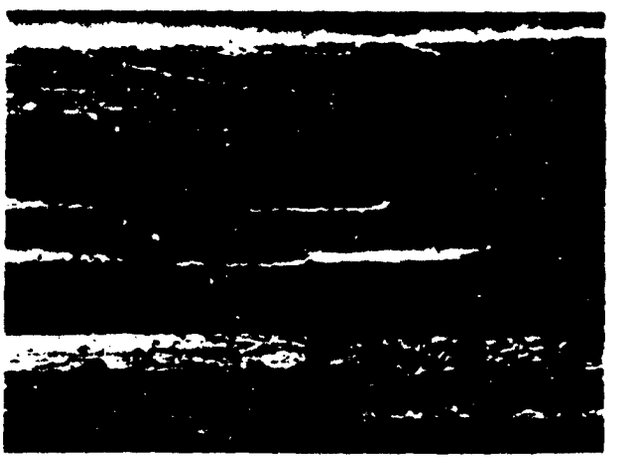

b

Figure 6. Virgin G/E Composite Before Test. (a) Edge View of "Circumferential" Orientation Specimen Showing Small Voids 20X. (b) Edge View of "Axial" Orientation Specimen Showing Elongated Voids 20X.

a

b

Figure 7. G/E Composite Showing Ply Boundaries. (a) Area Near Center of Specimen Showing Two Boundaries 100X. (b) Area Near Edge of Specimen Showing One Boundary 100X.

a

b

Figure 8. SEM Photomicrographs of Polished G/E Composite. (a) Fibers Running Parallel to the Surface 2000X. (b) Fibers Running Perpendicular To The Surface 2000X.

a

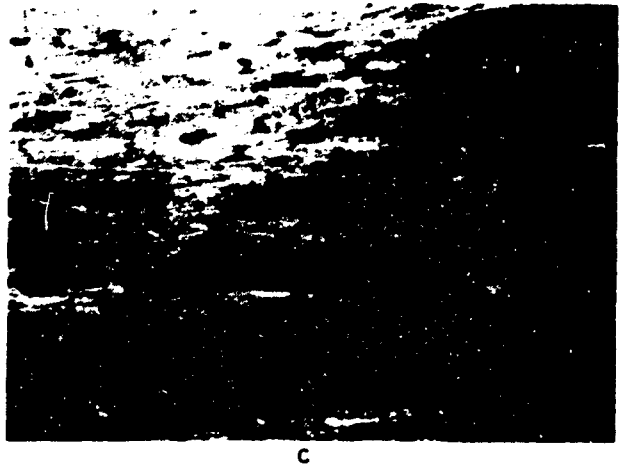

c

Figure 9. Virgin TWCP Before Test. (a) Edge View of Two "Axial" Orientation Specimens 3X. (b) Edge View of "Axial" Speciment 15X. (c) Edge View of "Circumferential" Orientation Specimen 15X.

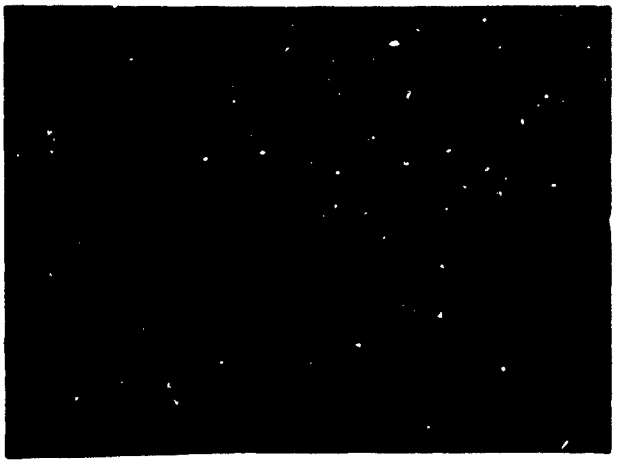

a

b

Figure 10. SEM Photomicrographs of Polished TWCP. (a) 500X. (b) 2000X.

SECTION IV

EXAMINATION OF DEGRADED G/E AND TWCP MATERIAL

Twelve specimens were used to produce the degraded sample of graphite/epoxy and TWCP. These specimens were all lay-ups of TWCP bonded to G/E with Silastic J adhesive. The dimensions were 10 mm of TWCP, 1 mm of Silastic J, and 3 mm of G/E. The specimen sizes used were 71 mm by 71 mm by 14 mm. Figure 11 is photographs of the specimens before impact with TWCP showing on top in 11a and G/E showing on top in 11b. All specimens were impacted on the TWCP side.

The twelve specimens were mechanically impacted in the Air Force Weapon's Laboratory's impact facility using the magnetic flyer. The conditions for each of the specimens are given in table 1, (taken from ref. 10). After impact, the specimens were examined with low power magnification to check for any damage. In addition, each specimen was checked for thickness growth after impact by measuring the thickness with a micrometer before and after impact. Most specimens were also checked for damage by ultrasonic techniques. Specimens which were impacted at the higher levels did show some damage at the edges. Figure 12 is a photograph of specimen 2 after impact. It shows two cracks in the G/E, one crack near the bond and one near the back surface. There is also a very small crack in the TWCP near the bond line. Figure 13 is a photograph of a specimen which had no apparent damage from impact (specimen 7). A porosity bubble in the Silastic J bond can be seen in figure 13. Such porosity was seen on some of the specimens.

After impact and subsequent examination, each impact specimen was sectioned into six bars for three point bend tests at Effects Technology, Inc. (ETI). Also, the G/E was separated from the TWCP by cutting through the Silastic J bond. After sectioning into beams, the edges of approximately one third of the specimens were polished and the beams sent to AFWL for microscopic examination. The remainder of the beams were visually examined at ETI. The results of the visual examination are given in Appendix I.

Microscopic examination of the G/E indicated that the edge cracking that was observed on the edges of the impact specimens did not extend very far into the center of the specimen. Figure 14 is a photograph of the end of a beam cut from impact specimen 2 (same as shown in figure 12). The crack of delamination

a

b

Figure 11. Specimens Used for Mechanical Impact. (a) View Showing TWCP on Top. (b) View Showing G/E On Top.

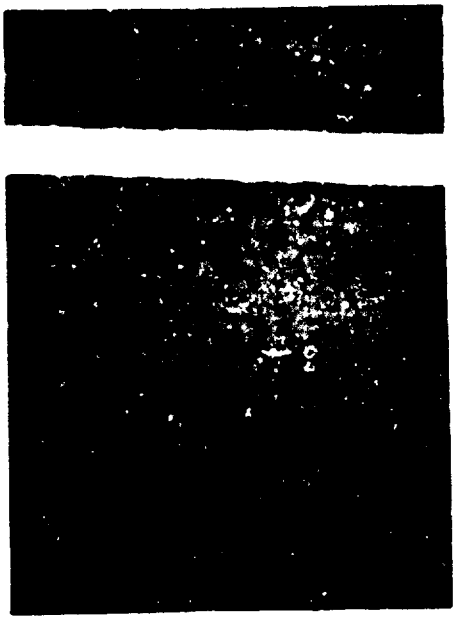

Figure 12. Specimen No. 2 After Impact. Note the Two Cracks in the G/E (on the right) and the Very Small Crack in the TWCP (on the left) 7X.

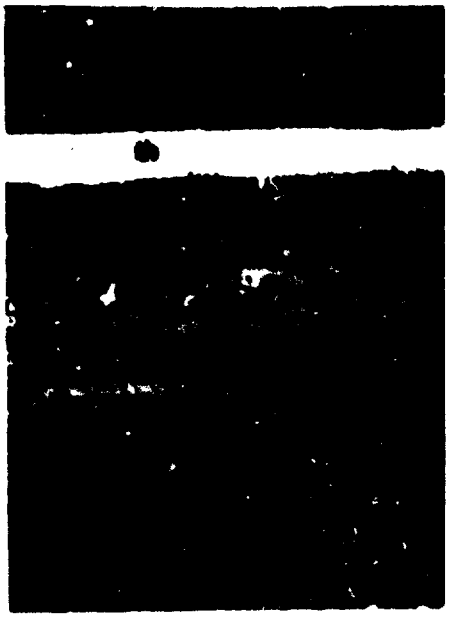

Figure 13. Specimen No. 7 After Impact. No Apparent Damage. Note Small Pore in Silastic J Bond (Middle White Layer) 7X.

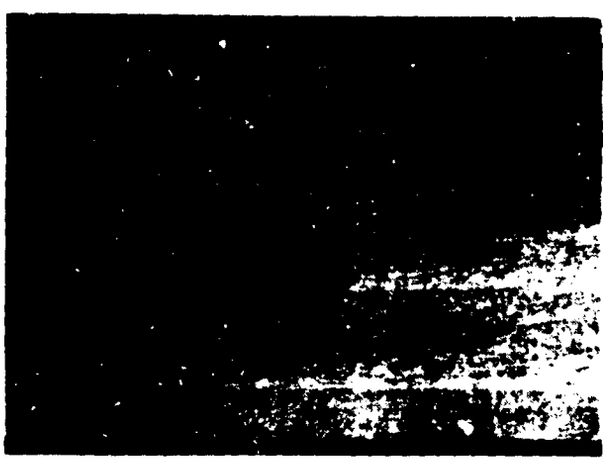

Figure 14. G/E Beam Cut From Specimen No. 2. Note that Crack (Same One That was Visible in figure 12) Does Not Extend Very Far Into Specimen 20X

Table 1

SPECIMEN DEGRADATION

Shot Number	Sample Number	Flyer[a] Thickness (mm)	Flyer Standoff (mm)	Flyer Impulse (ktap)	Total[b] Impulse (ktap)	Peak[c] Stress (kbar)	Results
1522	1	0.81	2.59	1.74	2.67	1.91	No apparent damage
1523	3	0.81	2.59	1.67	2.55	1.83	No apparent damage
1524	5	0.81	2.59	1.75	2.67	1.92	No apparent damage
1525	7	0.81	2.59	1.64	2.50	1.80	No apparent damage
1526	9	0.81	2.59	1.73	2.64	1.90	No apparent damage
1527	12	0.81	2.59	1.68	2.56	1.84	No apparent damage
1532	4	0.81	3.18	2.52	3.86	2.79	No apparent damage
1533	2	0.51	3.16	2.06	3.16	3.60	Visible crack in substructure, no separation
1540	6	0.51	3.16	1.69	2.58	2.95	No apparent damage
1541	8	0.51	3.16	1.69	2.58	2.95	Visible crack in substructure, no separation
1542	10	0.51	3.16	1.60	2.44	2.79	No apparent damage
1549	11	0.81	2.59	1.66	2.54	1.82[d] (1.75)	Transmitted stress measurement, see figure 9.

[a] All flyers were 1100-0 aluminum.

[b] Based on enhancement ratio of 1.53 from previous tests (Ktech TR76-09, Graphite-Resin Screening Tests, Nov 76)

[c] Impact stress calculated from a linear interpolation/extrapolation between calibration data and 0-impulse, 0-stress.

[d] Peak stress of 182 kbar was calculated, 1.75 kbar was measured.

ends a short distance from the end. Damage was observed on a few of the specimens near the center of the beams, but it is suspected that this occurred during separating the G/E from the TWCP because of the nature of such damage. It was generally concluded that damage to the G/E as a result of the mechanical impact was rather small and confined to the edges. No damage was detected (at least attributable to mechanical impact) on any specimen impacted at the lower levels.

On the TWCP on the other hand, virtually all of the specimens contained microcracks, whether impacted at the 200 MPa peak stress or 300 MPa peak stress. Only a couple of the polished specimens did not appear to have microcracks. Examples of microcracks in the TWCP can be seen in the photographs shown in figure 15. It was much more difficult to detect microcracks on the unpolished specimens so it is suspected that many of the TWCP specimens which were said to have "no visible damage" in Appendix I actually contained microcracks that would have been visible had the specimen been polished. It was therefore concluded that most, if not all, of the TWCP contained microcracks after being subjected to mechanical impact.

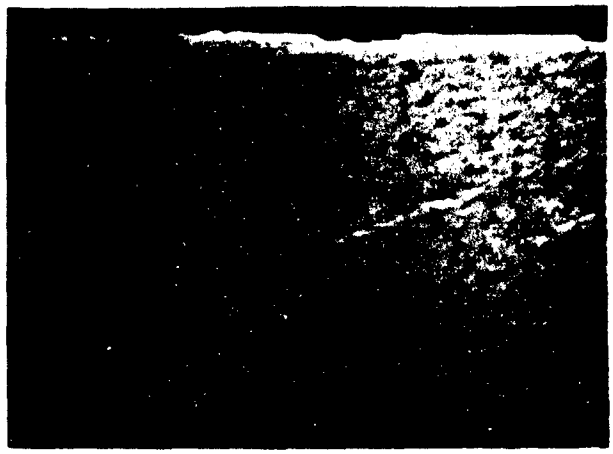

a

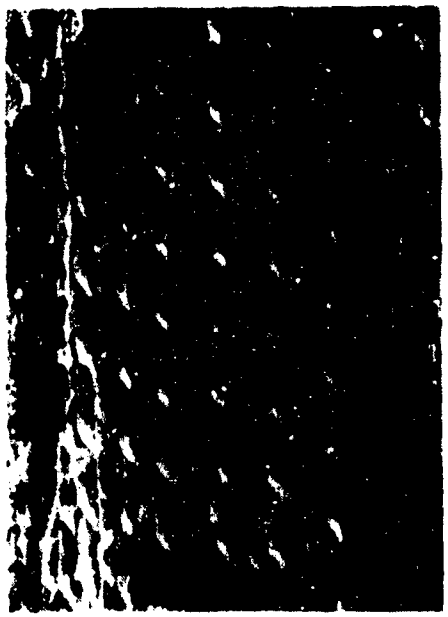

b

c

Figure 15. Edge Views of TWCP Beams After Mechanical Impact. (a) "Axial" Orientation Specimen Showing Diagonal Microcracks 6X. (b) "Circumferential" Specimen Showing Microcracks Parallel to the Surface 8X. (c) Higher Magnification of "Axial" Specimen 20X.

SECTION V

EXAMINATION OF G/E SPECIMENS AFTER THREE POINT BEND TEST

In examining the G/E specimens after being subjected to the three point bend test, the extreme conditions were chosen for study. Thus, the static test condition was looked at in each case and compared to the highest strain rate dynamic test ($\dot{\varepsilon}$ = 13 cm/sm/sec). Similarly, the specimens of virgin material were compared to those taken from the most severly degraded material (material which received the highest peak stress and/or impulse in the magnetic flyer). Since all the specimens of degraded material were 71 mm long, only the 71 mm long specimens of the virgin material were closely examined. A cursory examination of specimens of other lengths (51 and 127 mm) indicated that the fracture was not appreciably different from the 71 mm long specimens. In all test conditions, both the "axial" orientation where the outermost plies were aligned across the width of the specimen, and the "circumferential" orientation where the outermost plies were aligned along the length of the specimen were examined.

Visual examination of the specimens revealed that the "circumferential" specimens had less damage than the "axial" specimens. In the static test on the "circumferential" specimens, the outermost ply on the tensile side did not always fracture completely. As seen in figure 16, only a longitudinal split occurred on one specimen; on another, there was a transverse crack about one third of the way across the specimen, ending at a longitudinal split; and on the third "circumferential" specimen tested statically, there was a transverse crack across the specimen. All of the "circumferential" specimens tested statically had a transverse crack across the compression side of the specimen directly under where it was loaded. Two of these specimens appeared to have a fair amount of residual strength. Although the statically tested "circumferential" specimens had delamination, it was considerably less than most of the other specimens - less than all the "axial" specimens, and less than the "circumferential" specimens tested dynamically.

The dynamically tested "circumferential" specimens made of virgin material are shown in figure 17. In all of these specimens, the outermost fiber plies fractured and the specimens essentially broke into two parts although the two

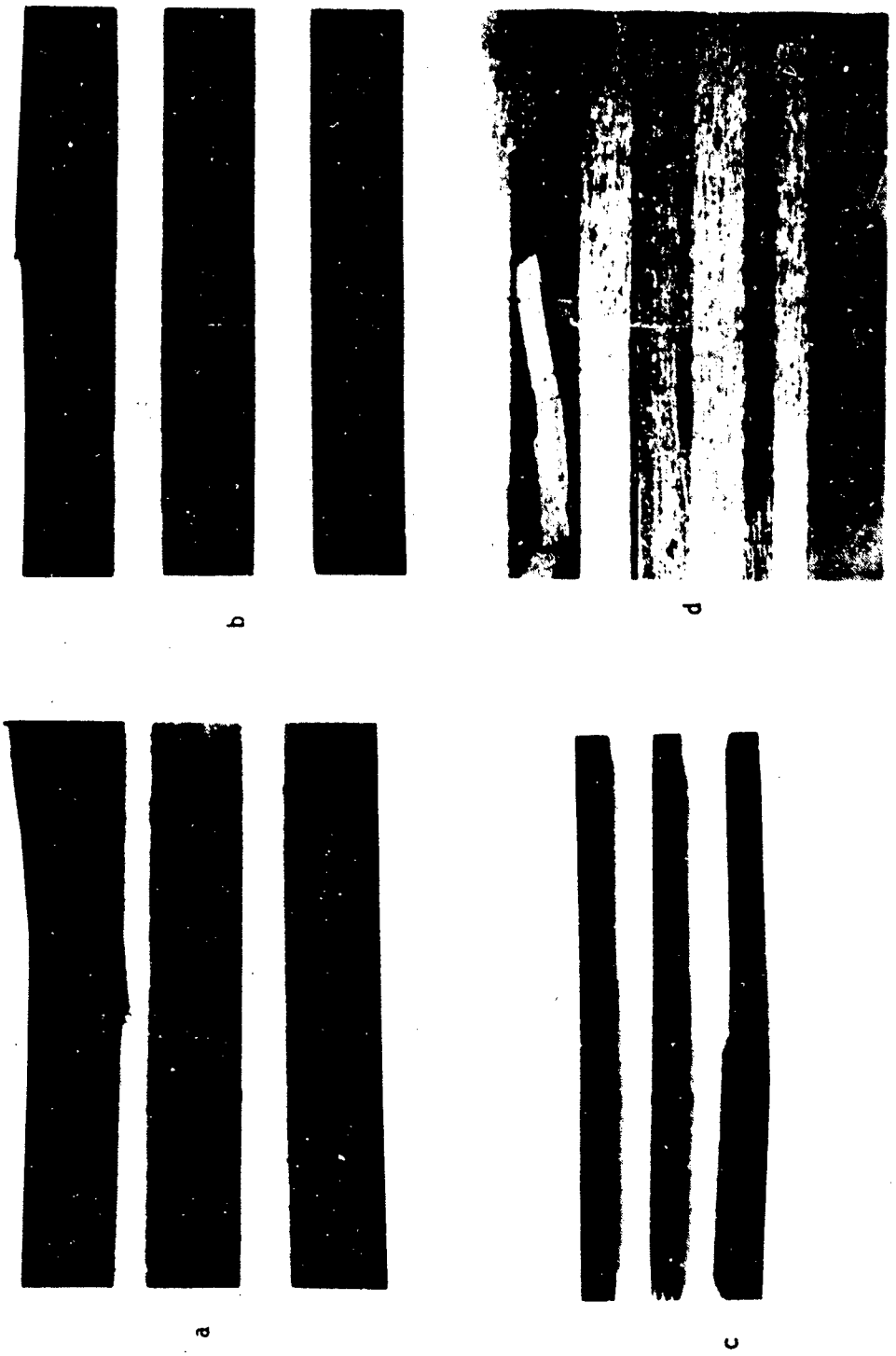

Figure 16. G/E Specimens After Test; Virgin Material, Static Test, "Circumferential" Orientation. (a) Tensile Side 2X. (b) Compression Side 2X. (c) Edge View 2X. (d) Edge View 20X.

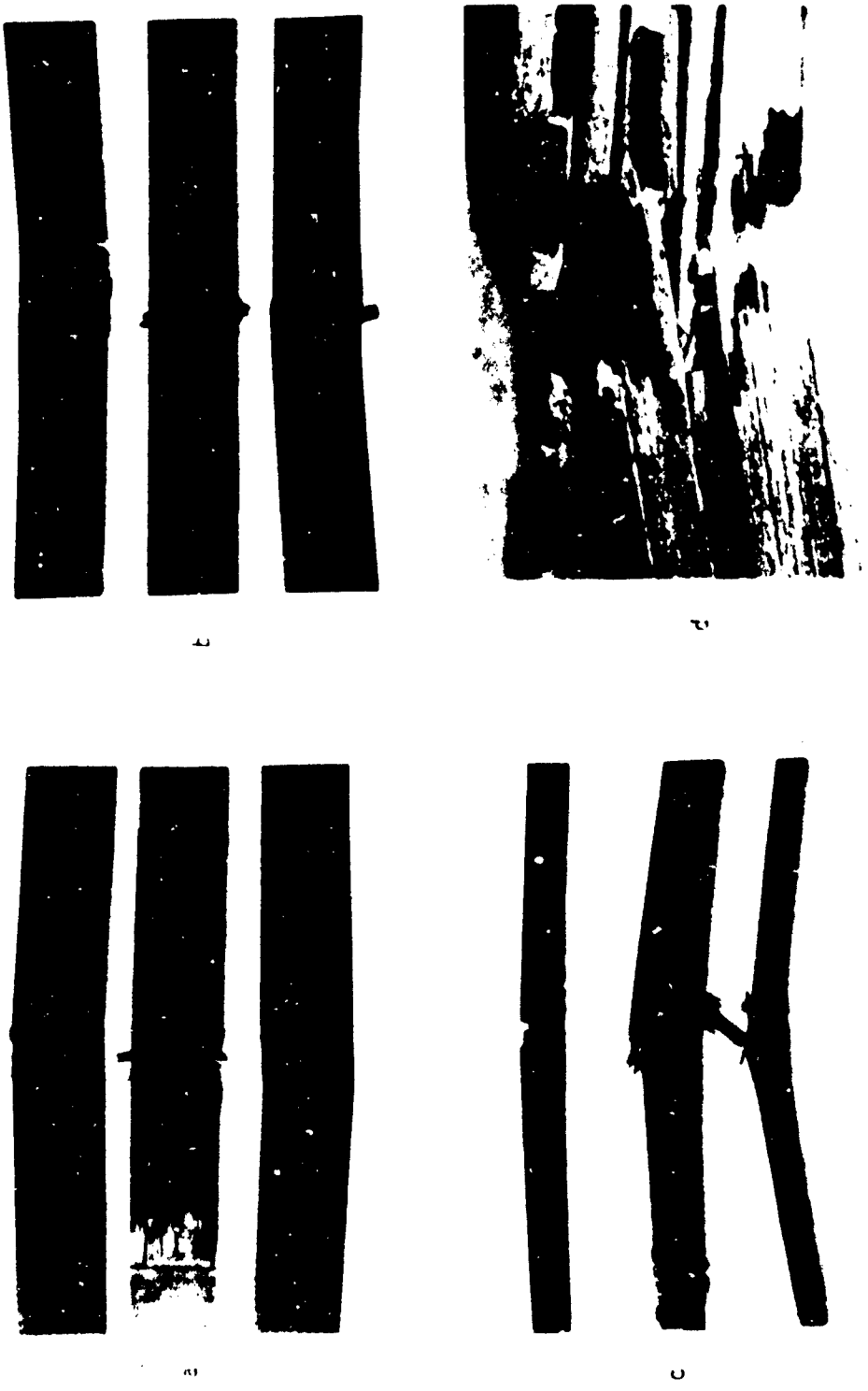

Figure 17. G/E Specimens After Test; Virgin Material, Dynamic Test, "Circumferential" Orientation. (a) Tensile Side 2X. (b) Compression Side 2X. (c) Edge View 2X. (d) Edge View 20X.

parts still hung lightly together. There appears to be finer delamination in the dynamically tested specimens versus the statically tested ones - compare figure 17d with figure 16d.

The statically tested "axial" specimens are shown in figure 18 and the dynamically tested "axial" specimens are shown in figure 19. There was not a substantial difference between the visual appearance of the statically tested and dynamically tested "axial" specimens. In all of the specimens, the outermost five plies (one layer of 90° and one layer of 0° plies) remained intact on the compression side and all of the remaining plies fractured. Again, there was a considerable amount of delamination which occurred on all specimens.

Samples which had been degraded by mechanical impact prior to test are shown in figures 20, 21, 22, and 23 after they had been tested. There appeared to be virtually no difference between the degraded specimens and the specimens made of virgin material. As in the virgin material, the specimens in the "circumferential" orientation broke with finer delaminations when tested dynamically than when tested statically - see figures 20b and 21b. There did not appear to be significant difference between the two test conditions in the "axial" specimens.

The scanning electron microscope (SEM) was used to look at the fracture surfaces at high magnification. For the G/E composites, both virgin and degraded material were examined after either static or dynamic tests. These four material/test condition combinations are shown in figures 24, 25, 26, and 27. A typical low magnification SEM photomicrograph of the fracture surface is shown in figure 28. By comparing similar areas from different test conditions, it can be seen that there is no significant difference from one test condition to another or from virgin material to degraded material. In comparing figure 24a, 25a, 26a, and 27a with each other, one can see that failure parallel to the fibers always occurred at or near the fiber-matrix interface (rather than entirely within the matrix) and that there was always a rather fine structure or "river" pattern in the fracture of the matrix. From figures 24b, 25b, 26b, and 27b, it can be seen that there is no significant difference in the fracture of the fibers themselves. Finally, from figures 24c and d, 25c and d, and 27c, it can be seen that fiber pullout was approximately the same in each test condition. Thus, it was concluded that there was no significant microscopic differences between the test conditions and degree of degradation of the

a

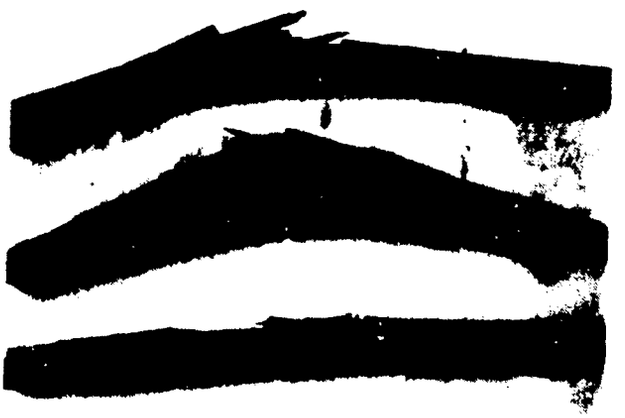

b

Figure 18. G/E Specimens After Test; Virgin Material, Static Test, "Axial" Orientation. (a) Tensile Side 2X. (b) Edge View 2X.

a

b

Figure 19. G/E Specimens After Test; Virgin Material, Dynamic Test, "Axial" Orientation. (a) Tensile Side 2X. (b) Edge View 2X.

a

b

Figure 20. G/E Specimens After Test; Degraded Material, Static Test, "Circumferential" Orientation. (a) Edge View 2X. (b) Edge View 10X.

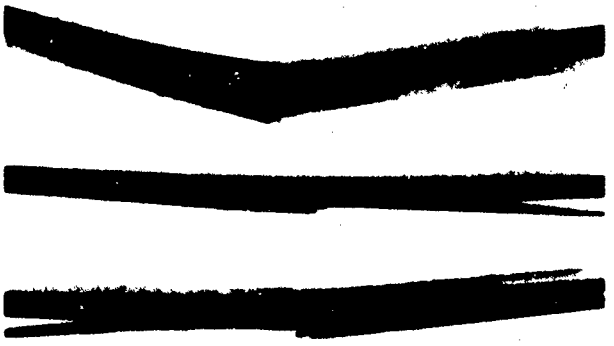

a

b

Figure 21. G/E Specimens After Test; Degraded Material, Dynamic Test, "Circumferential" Orientation. (a) Edge View 2X. (b) Edge View 10X.

a

Figure 22. G/E Specimens After Test; Degraded Material, Static Test, "Axial" Orientation. 2X.

b

Figure 23. G/E Specimens After Test; Degraded Material, Dynamic Test, "Axial" Orientation. 2X.

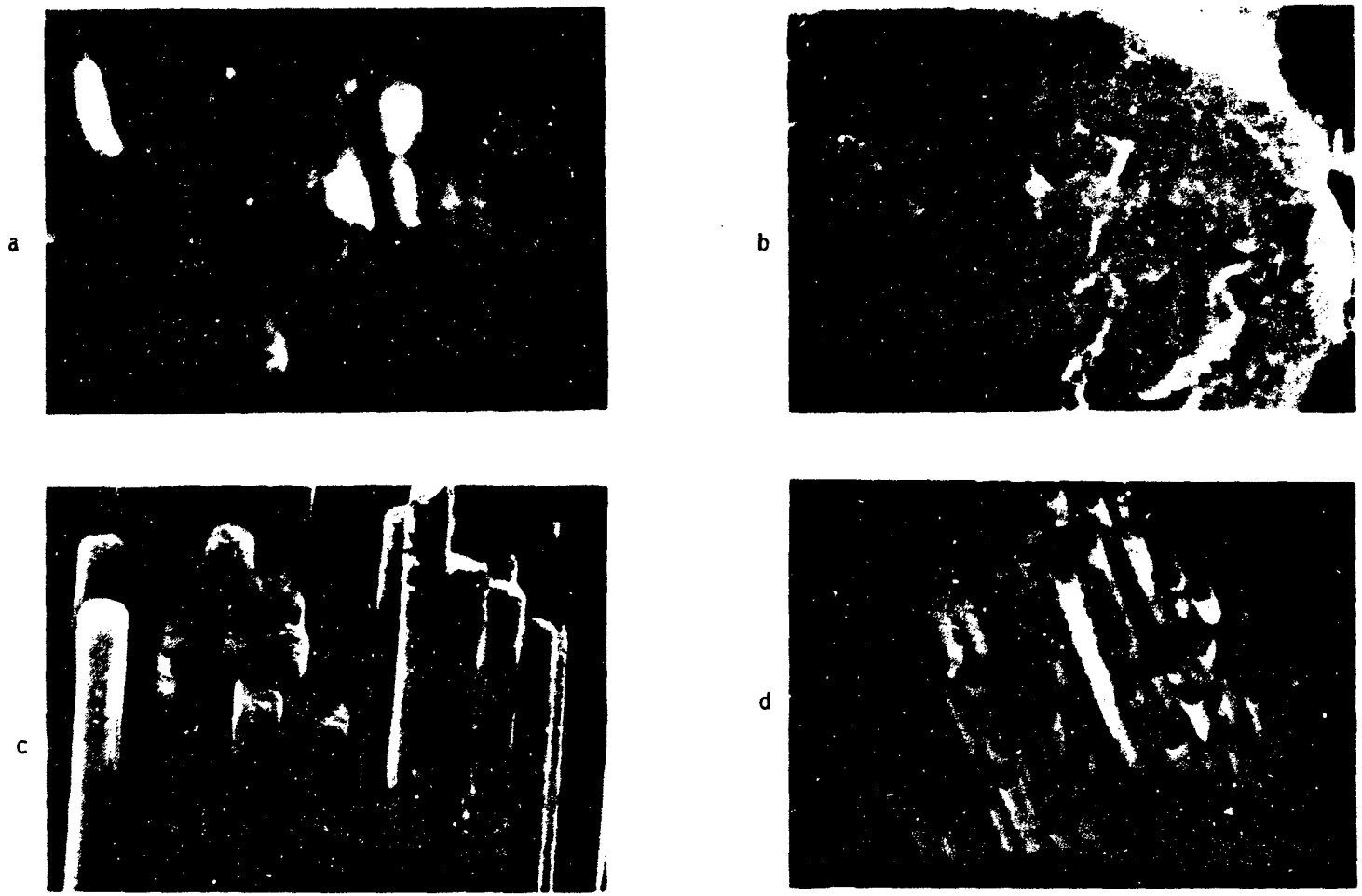

Figure 24. SEM Photomicrographs of Fracture Surfaces of G/E After Test; Virgin Material, Static Test. (a) View of Declamination Surface 2000X. (b) Single Fiber End 11500X. (c) Fiber End in 45° Ply 1000X. (d) Fiber Ends in Longitudinal Ply 500X.

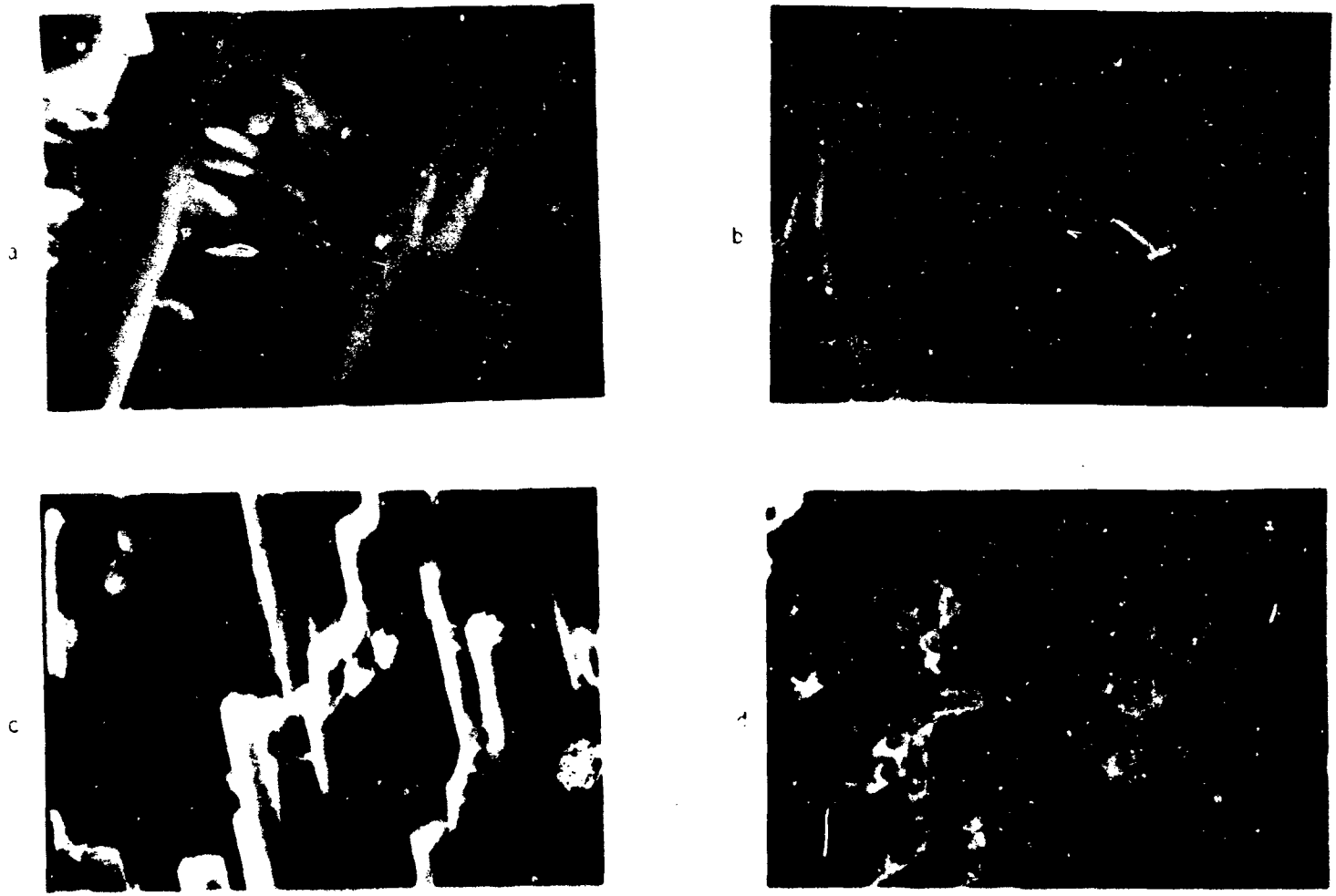

Figure 25. SEM Photomicrographs of Fracture Surfaces of G/E After Test; Virgin Material, Dynamic Test. (a) View of Delamination Surface 2000X. (b) Single Fiber End 11,500X. (c) Fiber Ends in 45° Ply 1000X. (d) Fiber Ends in Longitudinal Ply 500X.

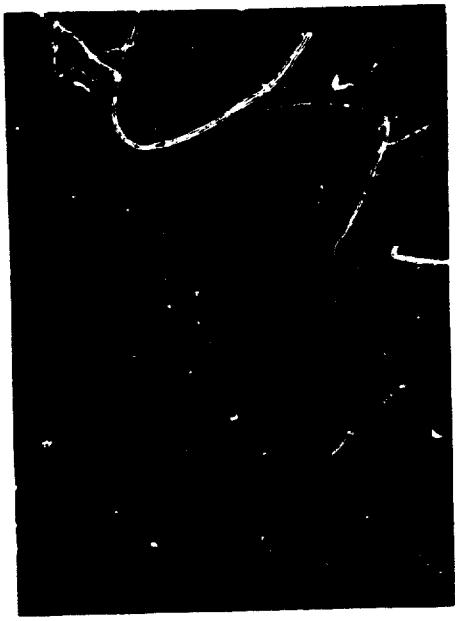

a

b

Figure 26. SEM Photomicrographs of Fracture Surfaces of G/E After Test: Degraded Material, Static Test. (a) View of Delamination Surface 220X. (b) Fiber Ends 660X.

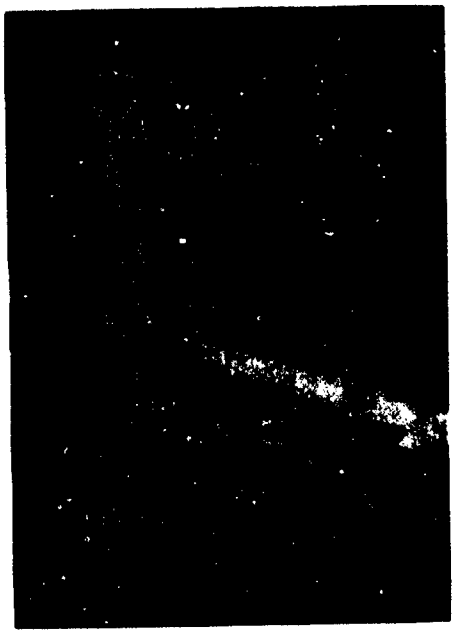

a

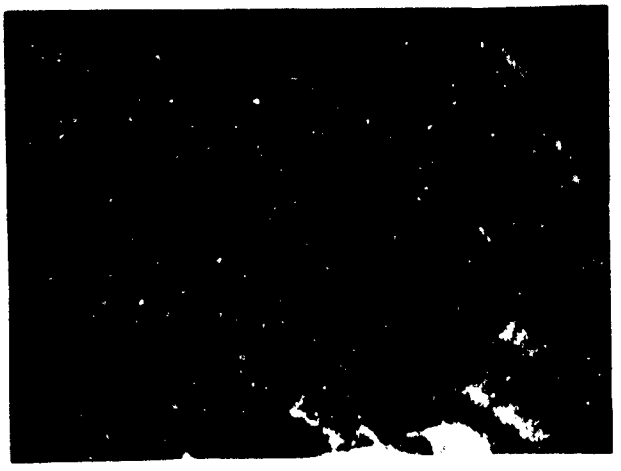

b

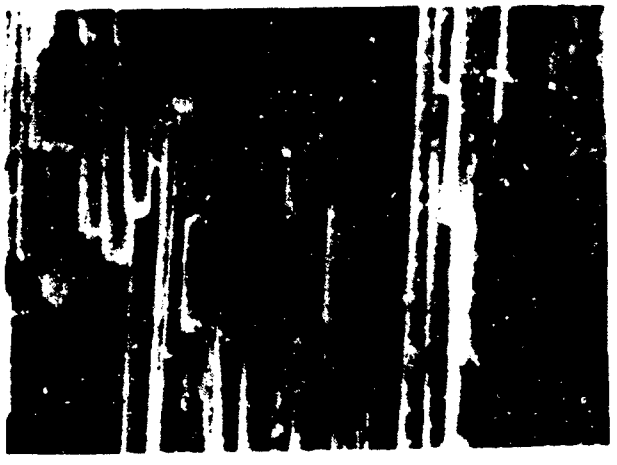

c

Figure 27. SEM Photomicrographs of Fracture Surfaces of G/E After Test; Degraded Material, Dynamic Test. (a) View of Delamination Surface 2000X. (b) Single Fiber End 11,500X. (c) Fiber Ends in 45° Plv 500X.

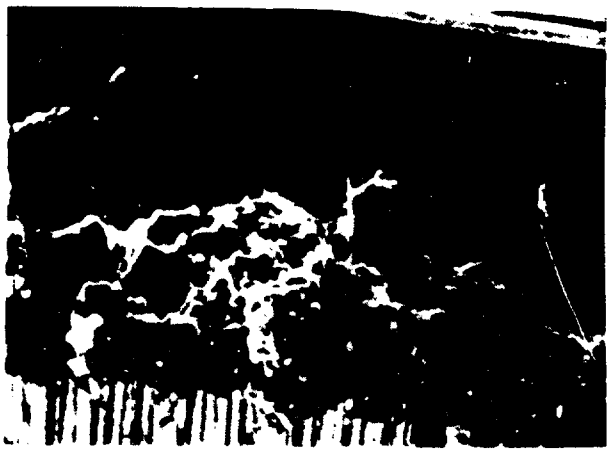

Figure 28. Typical Low Magnification SEM Picture of G/E Fracture Surface 200X.

material when tested. Similarly, there was no significant microscopic difference between specimens in the "axial" orientation and specimens in the "Circumferential" orientation. This correlated well with the test results of the G/E, (ref. 6).

SECTION VI

EXAMINATION OF TWCP AFTER THREE POINT BEND TEST

Tape Wrapped Carbon Phenolic (TWCP) specimens were examined after being subjected to the same test conditions as the G/E, i.e., the extreme strain rate test conditions and the extremes in preconditioning of the material were examined. The only difference between the TWCP and G/E test conditions was that the maximum strain rate ($\dot{\varepsilon}$ = 48 cm/cm/sec) was higher for the TWCP because of the greater thickness of the specimen (the velocity of the loading tup was the same in both cases). As in the case of the G/E, the only specimen length examined in detail were specimens 71 mm long. Specimens were cut in both the "axial" and "circumferential" orientations.

Photographs of the fractured TWCP specimens are shown in figures 29, 30, 31, and 32. As can be seen by comparing figure 29 with figure 30 or comparing figure 31 with figure 32, there is no apparent macroscopic difference between the statically tested and dynamically tested specimens. However, if one compares figure 29c with figure 31c or figure 30c with figure 32c, it can be seen that the fracture path followed a slightly different angle in the degraded material than in the virgin material. The angle (to the axis of the specimen) of the fracture path of the virgin material was 29 to 30° whereas the angle in the degraded material was 23° to 24°.

This difference in fracture angle between the virgin material is probably due to the presence of microcracks in the degraded material. Pre-test examination of the degraded material revealed microcracks in a majority of the specimens and it is felt that had the specimens been polished more an/or examined at higher magnification, microcracks would have been observed in all of the specimens. This material was laid up at a 20° angle of the plies to the axis and the interlaminar strength is the weakest. Thus, the angle of weakest material is 20°, but the angle of maximum stress in a three point bend test is 90° to the axis. Thus, the actual fracture path occurs somewhere between these two extremes and apparently resolved itself to approximately 30° for the virgin material. In the degraded material, on the other hand, microcracks formed on the interlaminar planes as a result of the one-dimensional shock loading from the simulated X-ray exposure. These microcracks made the already weakest plane

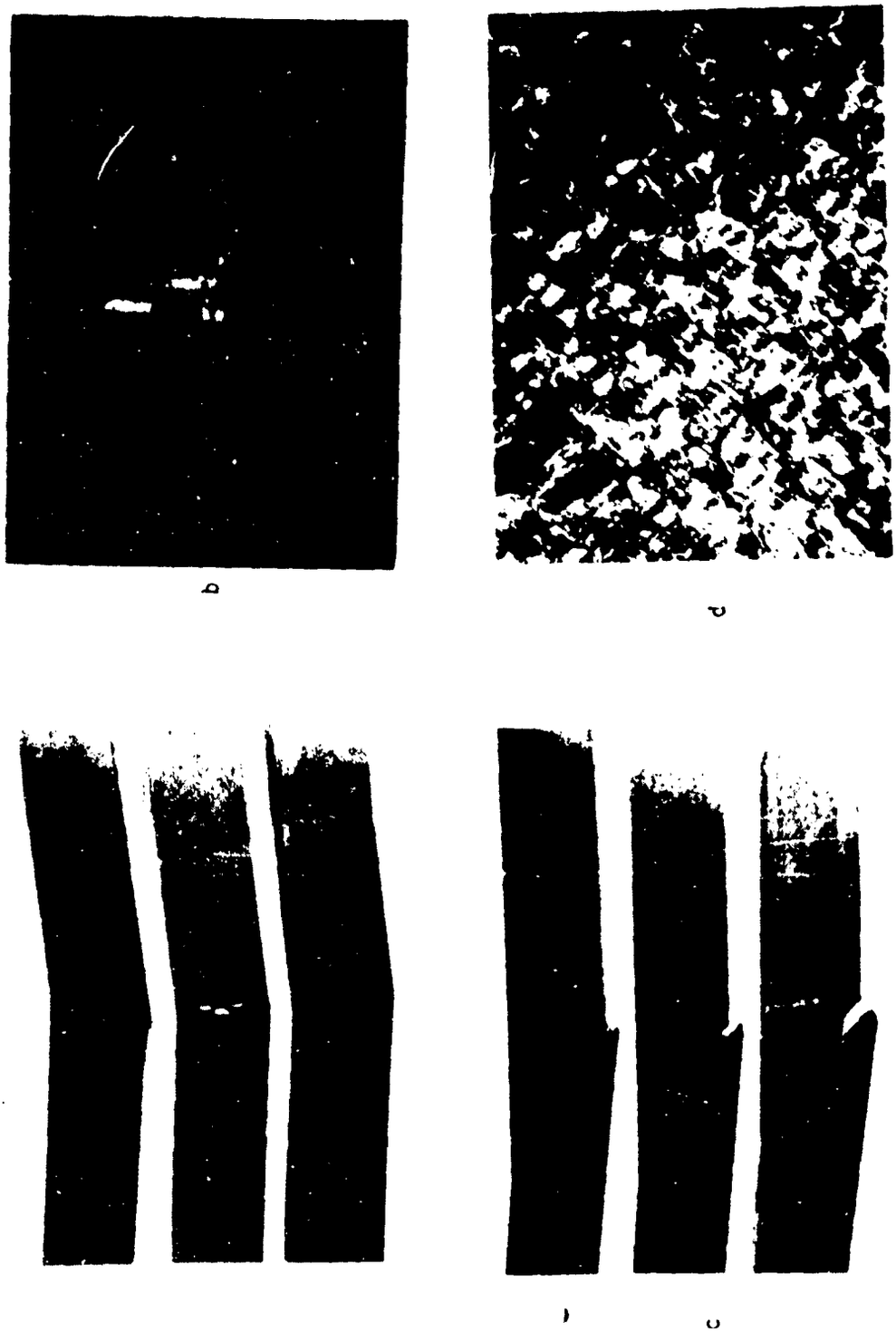

Figure 29. TWCP Specimens After Test; Virgin Material, Static Test. (a) Edge View of "Circumferential" Orientation Specimens 2X. (b) Closeup of (a) 8X. (c) Edge View of "Axial" Orientation Specimen 2X. (d) Fracture Surface of "Axial" Specimen 8X.

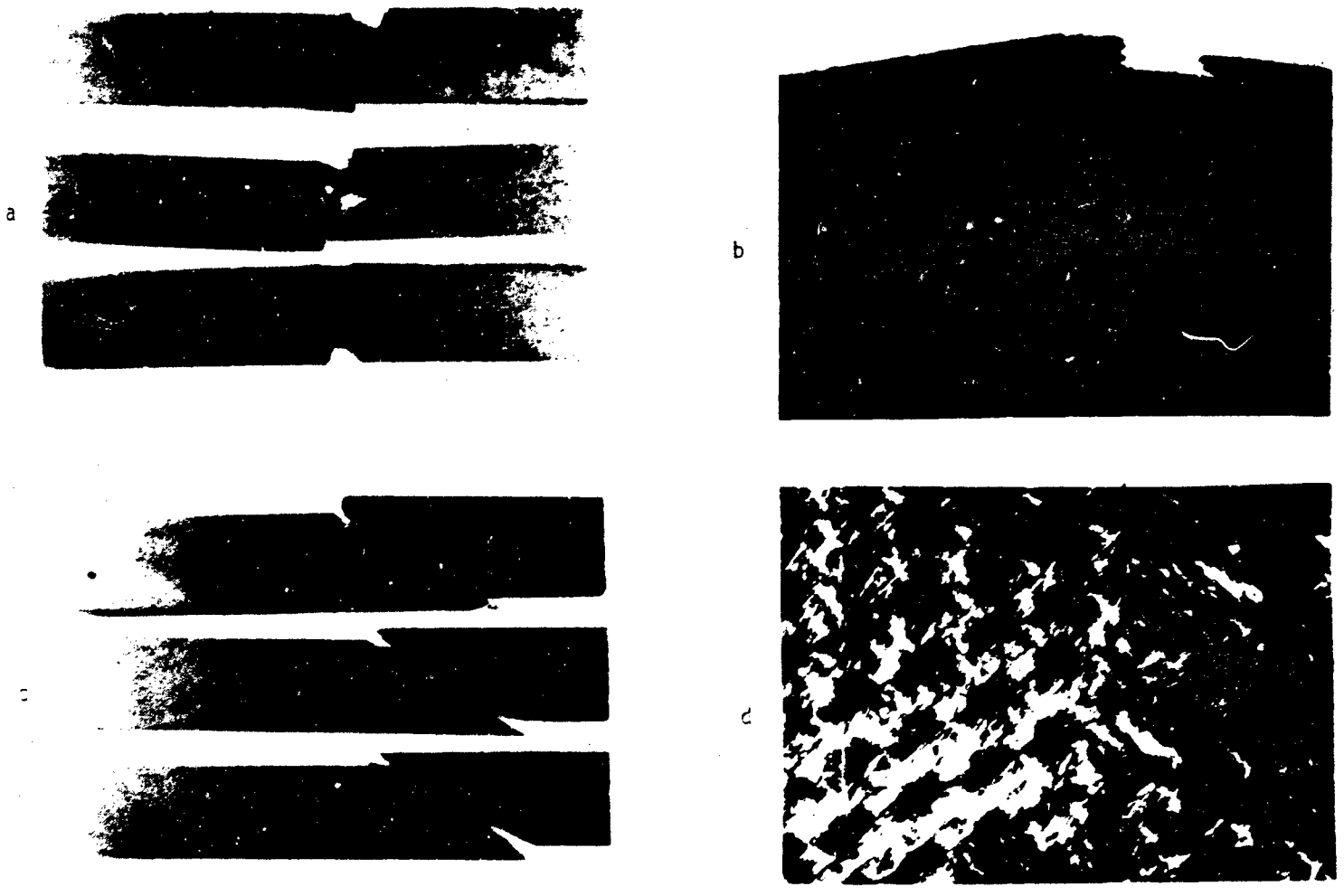

Figure 30. TWCP Specimens After Test; Virgin Material, Dynamic Test. (a) Edge View of "Circumferential" Orientation Specimens 2X. (b) Closeup of (a) 8X. (c) Edge View of "Axial" Orientation Specimen 2X. (d) Fracture Surface of "Axial" Specimen 8X.

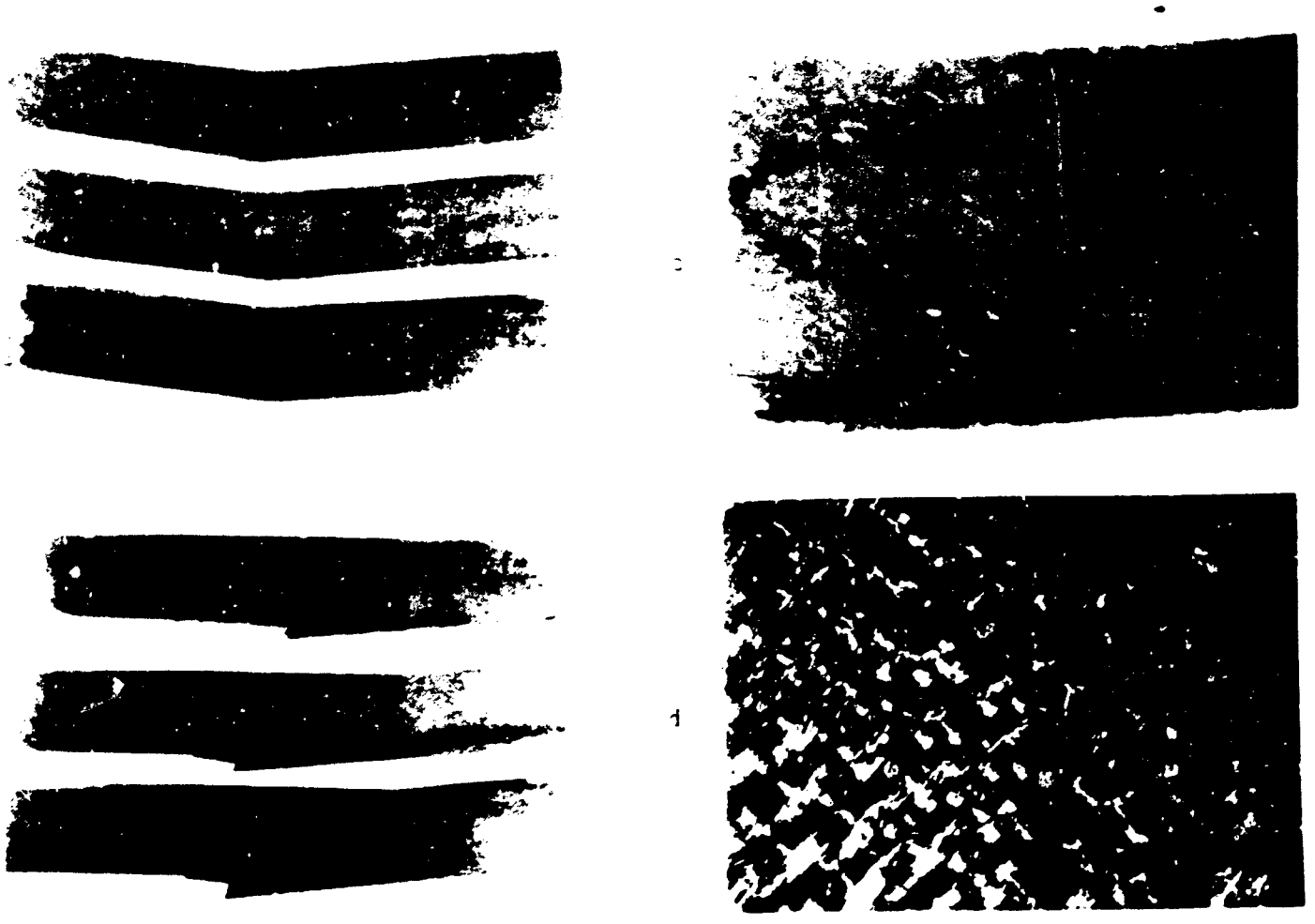

Figure 31. TWCP Specimens After Test; Degraded Material, Static Test. (a) Edge View of "Circumferential" Orientation Specimens 2X. (b) Closeup of (a) 8X. (c) Edge View of "Axial" Orientation Specimen 2X. (d) Fracture Surface of "Axial" Specimen 8X.

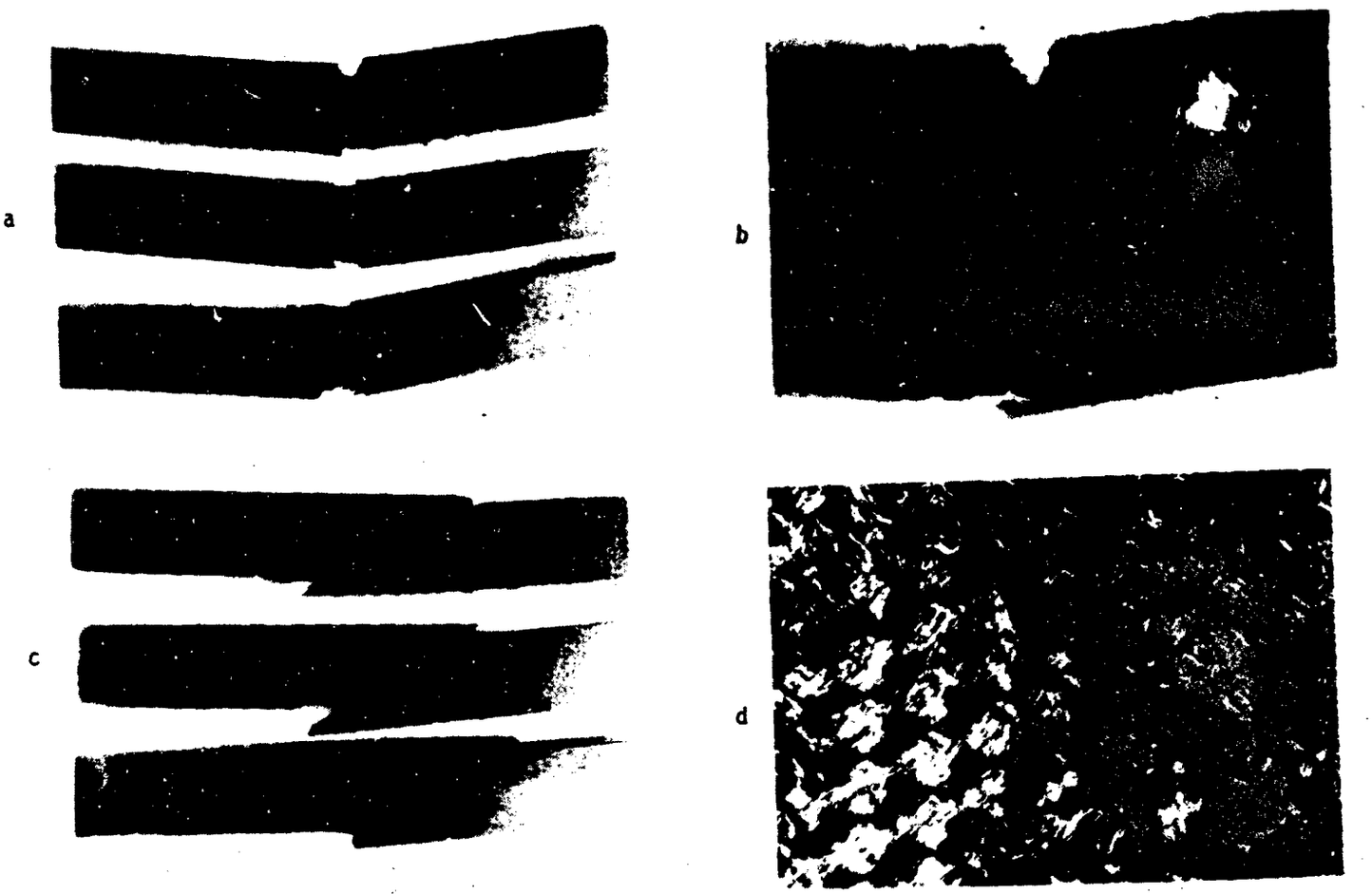

Figure 32. TWCP Specimens After Test; Degraded Material, Dynamic Test. (a) Edge View of "Circumferential" Orientation Specimens 2X. (b) Closeup of (a) 8X. (c) Edge View of "Axial" Orientation Specimen 2X. (d) Fracture Surface of "Axial" Specimen 8X.

still weaker. Thus, the fracture path would be expected to follow a path closer to the layup than it did in the virgin material. This agrees with the observed value of 23° to 24° for the degraded compared with 29° to 30° for the virgin material.

The fractured TWCP surfaces were also examined with the SEM. The results of this are shown in figures 33, 34, 35, and 36. In each case, a resin pocket (which represented but a small fraction of the fracture surface) is shown and a typical area of fibers is shown. As can be seen by comparing the various figures, no trend could be detected with either strain rate or degree of degradation - all surfaces appeared essentially the same at high magnifications.

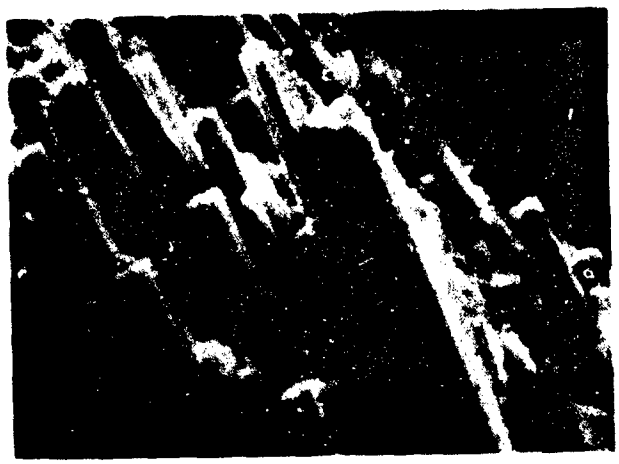

a

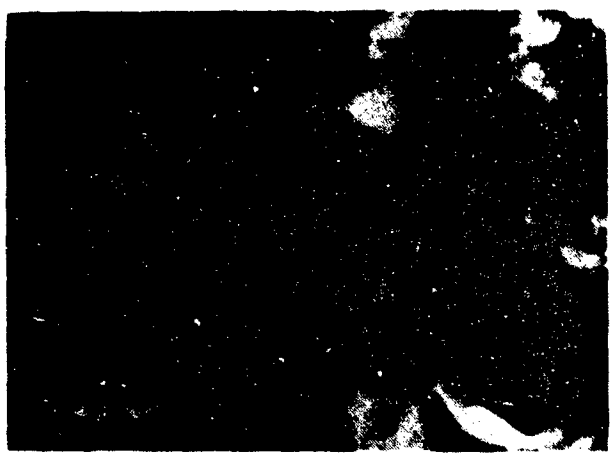

b

Figure 33. SEM Photomicrographs of Fracture Surfaces of TWCP After Test; Virgin Material, Static Test. (a) Fiber Area 500X. (b) Resin Area 2000X.

a

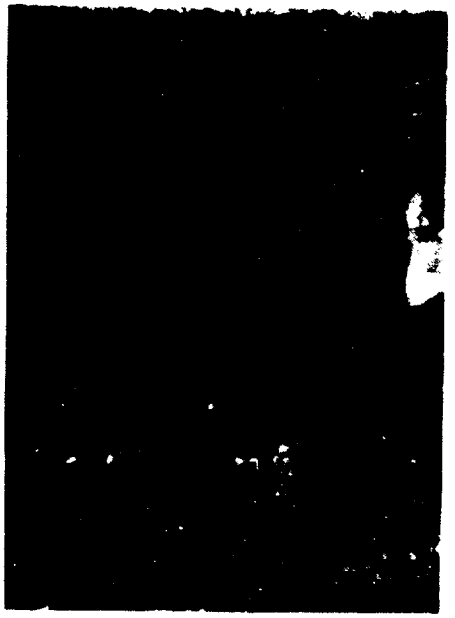

b

Figure 34. SEM Photomicrographs of Fracture Surfaces of TWCP After Test: Virgin Material, Dynamic Test. (a) Fiber Area 500X. (b) Resin Area 2000X.

a

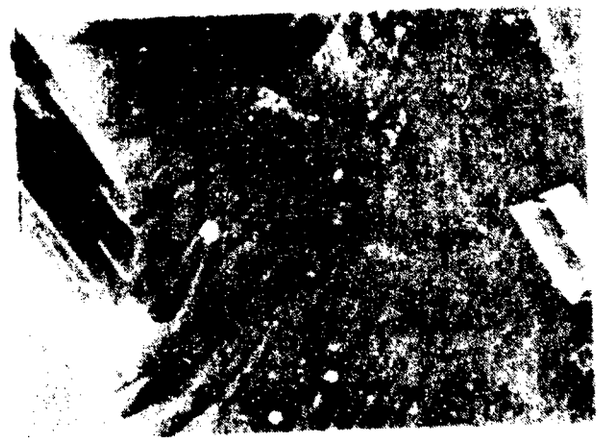

b

Figure 35. SEM Photomicrographs of Fracture Surfaces of TWCP After Test: Degraded Material, Static Test. (a) Fiber Area 500X. (b) Resin Area 2000X.

a

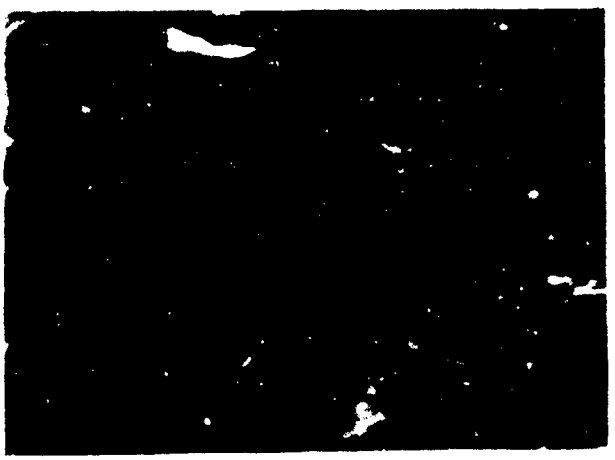

b

Figure 36. SEM Photomicrographs of Fracture Surfaces of TWCP After Test; Degraded Material, Dynamic Test. (a) Fiber Area 500X. (b) Resin Area 2000X.

SECTION VII

CONCLUSIONS

The following conclusions are drawn from the results of this investigation:

1. When differences are observed in the mechanical properties of a given material when tested at different strain rates, there is usually a difference in the appearance of the fracture surface.

2. Similarily, when no differences are observed in the mechanical properties of a given material when tested at different strain rates, then no differences will be observed in the fracture surfaces.

3. Differences which are observed in the fracture surfaces of a given material due to testing at different strain rates may be on a microscopic scale, a macroscopic scale, or both.

4. The fracture surfaces of the 3DQP had a different appearance when fractured at high strain rates versus low strain rates.

5. When subjected to a three point bend test, the G/E composite material failed with a large amount of delamination. Thus, extreme care must be used in interpreting the data obtained from this kind of test.

6. Little difference was observed in the fracture surfaces of TWCP fractured at various strain rates, but the angle of fracture on the "axial" orientation specimens was different for degraded material versus virgin material.

APPENDIX I

DDP

VISUAL INSPECTION (3X) OF DEGRADED TWCP & G/L

SPECIMEN	DEGRADATION CONDITION	TWCP	G/E
D1A2		NVD	Voids
D1A3	2 Kbar	NVD	NVD
D1A4	1.1 μsec	NVD	b-interlam. separation
D1A5		NVD	NVD
D3A1		NVD	NVD
D3A3	2 Kbar	NVD	NVD
D3A4	1.1 μsec	NVD	NVD
D3A6		NVD	NVD
D5A1		NVD	NVD
D5A2	2 Kbar	NVD	NVD
D5A5	1.1 μsec	NVD	NVD
D5A6		NVD	Voids - R
D7C2		NVD	poss. delam. T mid-plane
D7C3	2 Kbar	NVD	NVD
D7C4	1.1 μsec	NVD	NVD
D7C5		NVD	NVD
D9C1		NVD	NVD
D9C3	2 Kbar	NVD	debond (from mag flyer or clean up?) Tb
D9C4	1.1 μsec	NVD	debond (from mag flyer or clean up?) Tb
D9C6		NVD	incomplete ply-B-Tb
D12C1		NVD	NVD
D12C2	2 Kbar	NVD	small void (Tb)
D12C5	1.1 μsec	NVD	small voids T & B
D12C6		NVD	small voids - T

SPECIMEN	DEGRADATION CONDITION	TWCP	G/E
D6A2		possible cracks - Rb	NVD
D6A3	3 Kbar	possible crack - L&Rb	NVD
D6A4	0.7 μsec	possible crack - R-b	NVD
D6A5		NVD	NVD
D8A1		possible crack - b. R&L	voids L & R
D8A3	3 Kbar	cracks - b-R&L	voids L & R
D8A5	0.7 μsec	crack - b R & L	delam. - L & R
D8A6		possible crack - b-R (L too dark)	debond? - L
D10C2		NVD	NVD
D10C4	3 Kbar	NVD	NVD
D10C5	0.7 μsec	NVD	NVD
D10C6		NVD	NVD
D4A2		possible cracks - Lb	delam. starting - Rb
D4A3	2.8 Kbar	possible cracks R.L b	delam. starting - Lb
D4A4	1.1 μsec	NVD	NVD
D4A5		NVD	bondline crack? R
D2A1		NVD	NVD
D2A2	3.6 Kbar	hairline cracks - b	NVD
D2A4	.7 μsec	NVD	bondline crack
D2A6		hairline crack - L & R	void - L

Code: b - near bondline, NVD = no visible damage

T & B - Top and bottom of circum. specimens with specimen code as reference.

L & R - Left and right of axial specimens with specimen code as reference.

REFERENCES

1. Brown, James R. et al., Nondestructive, Thermal, and Mechanical Properties Evaluation of Composite Heatshield Materials, AFWL-TR-73-189, AFWL, Kirtland AFB, NM., January 1974.

2. Brown, James R., Jr., Sanders, H. G., and Pears, C. D., Nondestructive Evaluations of Composite Heatshield Materials Before and After an Underground Nuclear Exposure, AFWL-TR-73-247, AFWL, Kirtland AFB, NM., June 1974.

3. Lee, L. M., Shock Response of Panel-Moulded Carbon Phenolic, AFWL-TR-77-138, AFWL, Kirtland AFB, NM., to be published.

4. Tarbell, William W., Washington, Steven L., and Scammon, Richard J., Stress Wave Experiments on Quartz Phenolic Composite Materials, AFWL-TR-73-93, AFWL, Kirtland AFB, NM., September 1973.

5. Lee, L. M., Rice, D. A., and Stretanski, Shock Characterization of Three Dimensional Carbon and Quartz Composite Materials, AFWL-TR-75-270, AFWL, Kirtland AFB, NM, May 1976.

6. Globus, R, Van Blaricum, P., and Parisse, R., Dynamic and Degraded Properties of Reentry Materials, SAMSO-TR-77-90, Vol 15, SAMSO, Los Angeles Air Force Station, Los Angeles, CA, to be published.

7. Adams, D.F. and Perry, J. L., "Static and Impact Behavior of Graphite/Epoxy Composite Laminates Containing Third-Phase Reinforcement Materials," Journal of Testing and Evaluation, Vol. 5, No. 2, March 1977, pp. 114-123.

8. Perry, J.L., Kirkhart, J.L., and Adams, D.F., Third-Phase Fiber Addition to Advanced Graphite Composites for Improvement of Impact Strength, Final Report, Naval Air Systems Command Contract N0019-73-C-0389, (AD 777074), Washington, DC., March 1974.

9. Perry, J.L., Adams, D.F., and Miller, A.K., Effect of Low Level Impact on Advanced Composites, Final Report, Naval Air Systems Command Contract N00019-74-C-0229 (AD A004470), Washington, DC, January 1975.

10. Brooks, A. L., Dynamic/Degraded Properties Test Program, Ktech Corp. TR77-02, Albuquerque, NM., April 1977.

LIST OF ACRONYMS

AFWL	Air Force Weapons Laboratory
DDP	Dynamic/Degraded Properties Program
DYV	Environment and Effects Branch of AFWL
ETI	Effects Technology, Incorporated
G/E	Graphite Epoxy Composite
RV	Reentry Vehicle
SAMSO/ABRES	Space and Missile Systems Organization/ Advanced Ballistic Reentry Systems Deputate
SEM	Scanning Electron Microscopy
3DQP	Three-dimensional Quartz Phenolic
TWCP	Tape Wrapped Carbon Phenolic
V & H	Vulnerability and Hardness

DISTRIBUTION

DNA/SPAS/WashDC
SAMSO/ABRES/RSSE/Los Angeles, CA
AFML/MBC/WPAFB, OH
AFWL/DYV/KAFB, NM
AFWL/SUL/KAFB, NM
AFWL/HO/KAFB, NM
AVCO Corp/Wilmington, MA
Ktech Corp/Albuquerque, NM
Effects Technology, Inc., Santa Barbara, CA
McDonnell/Douglas Astro Co/Huntington Beach, CA
Systems, Science, Software, La Jolla, CA
Southern Rsch Inst/Burmingham, AL
AUL/LDE/Maxwell AFB, AL
DDC/TCA/Cameron Sta/Alexandria, VA
Official Record Copy/AFWL/DYV